

Quantum and thermal Casimir interaction between a sphere and a plate: Comparison of Drude and plasma models

Roya Zandi,¹ Thorsten Emig,^{2,3} and Umar Mohideen¹

¹*Department of Physics and Astronomy, University of California, Riverside, California 92521, USA*

²*Institut für Theoretische Physik, Universität zu Köln, Zùlpicher Strasse 77, 50937 Köln, Germany*

³*Laboratoire de Physique Théorique et Modèles Statistiques, CNRS UMR 8626, Université Paris-Sud, 91405 Orsay, France*

(Received 27 February 2010; revised manuscript received 21 April 2010; published 17 May 2010)

We calculate the Casimir interaction between a sphere and a plate, both described by the plasma model, the Drude model, or generalizations of the two models. We compare the results at both zero and finite temperatures. At asymptotically large separations we obtain analytical results for the interaction that reveal a nonuniversal, i.e., material-dependent interaction for the plasma model. The latter result contains the asymptotic interaction for Drude metals and perfect reflectors as different but universal limiting cases. This observation is related to the screening of a static magnetic field by a London superconductor. For small separations we find corrections to the proximity force approximation that support correlations between geometry and material properties that are not captured by the Lifshitz theory. Our results at finite temperatures reveal for Drude metals a nonmonotonic temperature dependence of the Casimir free energy and a negative entropy over a sizeable range of separations.

DOI: [10.1103/PhysRevB.81.195423](https://doi.org/10.1103/PhysRevB.81.195423)

PACS number(s): 03.70.+k, 12.20.-m

I. INTRODUCTION

The past decade has witnessed rapid progress in the precision of Casimir force measurements.¹⁻⁶ The measurement precision that is expected in the near future demands accurate theoretical calculations of the Casimir force for the geometries and materials used in experiments. While Casimir's original calculation for perfect metal plates⁷ and Lifshitz's formula for dielectric slabs⁸ only apply to planar, parallel surfaces, recent measurements have set limits on geometry-induced corrections in the most frequently used sphere-plate geometry.⁹ The geometry dependence of Casimir forces is intriguing as it can vary substantially with the shape and relative orientation of the objects.¹⁰⁻¹² Material dependence in the form of dissipation of conduction electrons has been experimentally confirmed to have an effect on the Casimir force.^{5,13} It is thus important that the geometry and material dependence be carefully investigated for the experimentally most important sphere-plate configuration.

In order to compare the experimental results to theory, the Derjaguin or proximity force approximation (PFA) (Ref. 14) has commonly been used. This approximation neglects the nonadditivity of Casimir forces by estimating the interaction between curved surfaces in terms of the planar surface interaction between infinitesimal and parallel surface elements. Its validity is hence limited to the singular limit of vanishingly small separations between the surfaces. A systematic extension to larger separations is not possible within such approximations.

The first exact computation of the Casimir interaction energy for a perfectly reflecting sphere and plate was presented in Ref. 15. Recently, corrections that come from using the plasma or Drude model were computed at zero temperature¹⁶ and at $T=300$ K.¹⁷ Other open geometries with curvature such as a cylinder above a plate have been studied for perfect metals.¹⁸ Corrections to the PFA in the case of perfect metals for a cylinder above a plate and a sphere above a plate have

been obtained using path-integral approaches^{19,20} and for scalar fields employing a world line formalism.²¹

Here we show that Casimir forces reveal a rich interplay between geometry (radius of the sphere and object's separation), optical properties of metals and thermal fluctuations. We study this in detail by calculating the Casimir interaction for different sphere radii and separations using the (i) the Drude model, (ii) a generalized Drude model, (iii) the plasma model, and (iv) a generalized plasma model at different temperatures. The study of these combined effects is of utmost importance since Casimir force measurements continue to be carried out using this geometry and an increasing accuracy is expected. Hence, the experimental findings will begin to show sensitivity to the material and temperature effects, which we take into account here. Furthermore, the unabated controversy whether the plasma or the Drude model is more appropriate for describing the optical properties of metals in Casimir calculations compels us to provide results for both models so that experimentalists can build on them when studying this problem further. The plasma model is a high-frequency description of the optical properties and the divergence $\sim 1/\omega^2$ of its dielectric function for small ω is unphysical for metals. The Drude model provides a proper low-frequency description for metals with a $1/\omega$ divergence of the dielectric function for small ω . At large frequencies, both models become identical.

Below, we supply numerical results for the Casimir interaction at arbitrary separations as well as analytic formulas for the asymptotic interaction at large separations. Depending on the model under consideration, the asymptotic results show universal or nonuniversal (i.e., material-independent or -dependent) behavior, a feature which is not present for the simple case of two parallel metal plates and hence results from the interplay of finite object sizes and material properties.

II. GENERAL EXPRESSION FOR THE INTERACTION

To calculate the interaction of a metallic sphere of radius R and a metallic plate with a separation d between the center of the sphere and the plate, we employ a scattering approach for Casimir interactions, which is described in detail in Ref. 11. The Casimir free energy of this system at temperature T is given by

$$E = k_B T \sum'_{n=0} \log \det[1 - Y(\kappa_n)] \quad (1)$$

with Matsubara wave numbers $\kappa_n = 2\pi n k_B T / \hbar c$. The primed sum indicates that the contribution for $n=0$ is to be weighted by a factor of $1/2$. At zero temperature the sum is replaced by an integral along the imaginary frequency axis,¹¹

$$T_{s,lm}^M = \frac{\pi}{2} \frac{\eta I_{l+1/2}(\kappa R) [I_{l+1/2}(n\kappa R) + 2n\kappa R I'_{l+1/2}(n\kappa R)] - n I_{l+1/2}(n\kappa R) [I_{l+1/2}(\kappa R) + 2\kappa R I'_{l+1/2}(\kappa R)]}{\eta K_{l+1/2}(\kappa R) [I_{l+1/2}(n\kappa R) + 2n\kappa R I'_{l+1/2}(n\kappa R)] - n I_{l+1/2}(n\kappa R) [K_{l+1/2}(\kappa R) + 2\kappa R K'_{l+1/2}(\kappa R)]} \quad (4)$$

with $n = \sqrt{\epsilon(ick)\mu(ick)}$, $\eta = \sqrt{\epsilon(ick)/\mu(ick)}$. These elements are also known as Mie coefficients.²² The T -matrix elements for E multipoles, $T_{s,lm}^E$, are obtained from Eq. (4) by interchanging ϵ and μ and by changing the overall sign. By taking $\epsilon(ick) \rightarrow \infty$ at an arbitrarily fixed $\mu(ick)$ in Eq. (4), the limit of a perfectly reflecting sphere and plate is obtained. Then the matrix elements become independent of μ ,

$$T_{s,lm}^M = \frac{\pi}{2} \frac{I_{l+1/2}(\kappa R)}{K_{l+1/2}(\kappa R)}, \quad (5a)$$

$$T_{s,lm}^E = -\frac{\pi}{2} \frac{I_{l+1/2}(\kappa R) + 2\kappa R I'_{l+1/2}(\kappa R)}{K_{l+1/2}(\kappa R) + 2\kappa R K'_{l+1/2}(\kappa R)}. \quad (5b)$$

These matrix elements scale for small κ as κ^{2l+1} . It is interesting to compare this behavior to the scaling of the general matrix elements of Eq. (4) for the dielectric functions of the Drude and plasma model. For both models the $T_{s,lm}^E \sim \kappa^{2l+1}$ behavior is unchanged for E multipoles. The coefficients become material (plasma frequency) dependent for the plasma model but retain the universal values of a perfect reflector for the Drude model. However, for M multipoles only the plasma model shows this universal behavior while the Drude model yields a different scaling $T_{s,lm}^M \sim \kappa^{2l+2}$ with nonuniversal conductivity-dependent coefficients.

The operator U can also be expressed in a spherical wave basis. It describes the propagation of waves from the sphere to the plate, a reflection at the plate, and the propagation back to the sphere. The reflection of waves at a dielectric plane is described most easily in a plane-wave basis with in-plane wave vector k_{\parallel} . The T -matrix elements of the plane are then given by the usual Fresnel coefficients. The conversion from plane to spherical waves and simultaneous translation from the sphere to the plane is obtained by multiplying

$$E = \frac{\hbar c}{2\pi} \int_0^{\infty} d\kappa \log \det[1 - Y(\kappa)], \quad (2)$$

where the matrix Y is given by the product

$$Y_{lml'm'}^{\alpha\beta} = T_{s,lm}^{\alpha} U_{lml'm}^{\alpha\beta} \delta_{mm'} \quad (3)$$

of the T operator T_s of the sphere and an operator U that describes the propagation of waves between the plate and the sphere and the scattering of them at the plate (see below). We represent these operators in a vector basis of spherical waves, where $\alpha, \beta = E, M$ denote electric or magnetic multipoles and l, m label the spherical waves. For a sphere of radius R with uniform permittivity $\epsilon(\omega)$ and permeability $\mu(\omega)$ the T -matrix elements for M multipoles are given by

the plane's T matrix from left and right by a matrix $D_{lm}^{\alpha\beta}(k_{\parallel})$. After defining $z = k_{\parallel} / \kappa$, the matrix multiplication runs over the continuous variable z and the elements of the operator U can be written as

$$U_{lml'm}^{\alpha\beta} = \int_0^{\infty} \frac{z dz}{4\pi} \frac{e^{-2d\kappa\sqrt{1+z^2}}}{\sqrt{1+z^2}} \sum_{\gamma} D_{lm}^{\alpha\gamma}(z) T_p^{\gamma}(\kappa, z) D_{l'm}^{\beta\gamma*}(z), \quad (6)$$

where the plate's diagonal T matrix, $T_p^{\gamma}(\kappa, z)$, for polarization γ are given by

$$T_p^M = -\frac{\mu(ick)\sqrt{1+z^2} - \sqrt{\epsilon(ick)\mu(ick) + z^2}}{\mu(ick)\sqrt{1+z^2} + \sqrt{\epsilon(ick)\mu(ick) + z^2}}, \quad (7a)$$

$$T_p^E = \frac{\epsilon(ick)\sqrt{1+z^2} - \sqrt{\epsilon(ick)\mu(ick) + z^2}}{\epsilon(ick)\sqrt{1+z^2} + \sqrt{\epsilon(ick)\mu(ick) + z^2}}. \quad (7b)$$

The exponential factor in Eq. (6) describes the translation from the sphere to the plane and back by a total distance $2d$ in the plane-wave basis. The elements of the matrix that converts between plane and spherical waves are given by

$$D_{lm}^{MM} = D_{lm}^{EE} = \sqrt{\frac{4\pi(2l+1)(l-m)!}{l(l+1)(l+m)!}} z P_l^{m'}(\sqrt{1+z^2}), \quad (8a)$$

$$D_{lm}^{EM} = -D_{lm}^{ME} = \sqrt{\frac{4\pi(2l+1)(l-m)!}{l(l+1)(l+m)!}} \frac{im}{z} P_l^m(\sqrt{1+z^2}), \quad (8b)$$

where P_l^m is the associated Legendre polynomial of order l , m . These elements have the following symmetries under complex conjugation,

$$D_{lm}^{\alpha\alpha^*} = (-1)^m D_{lm}^{\alpha\alpha}, \quad (9a)$$

$$D_{lm}^{\text{ME}^*} = (-1)^{m+1} D_{lm}^{\text{ME}}. \quad (9b)$$

In what follows we employ Eqs. (1) and (2) to obtain the Casimir interaction for perfectly reflecting bodies and also for metals described by the plasma and Drude model at zero and finite temperatures.

III. LARGE DISTANCE INTERACTION AT $T=0$

In this section we consider the zero-temperature Casimir interaction at large separations for different dielectric functions.

A. Perfect reflector

In the limit of perfect reflectivity of the plate, one finds from Eq. (6) with $\epsilon \rightarrow \infty$ the simple T -matrix elements $T_p^{\text{M}} = T_p^{\text{E}} = 1$. With this simplification, the integration over z in Eq. (6) can be performed analytically. We find for the elements of U the same result that was obtained before, using the method of images,¹⁵

$$U_{lm'l'm}^{\text{MM}} = U_{lm'l'm}^{\text{EE}} = (-1)^{l+l'+1} \sum_{l''=|l-l'|}^{l+l'} \frac{(-1)^{l''}}{2} [l(l+1) + l'(l'+1) - l''(l''+1)] \sqrt{\frac{(2l+1)(2l'+1)}{l(l+1)l'(l'+1)}} (2l''+1) \times \begin{pmatrix} l' & l & l'' \\ 0 & 0 & 0 \end{pmatrix} \begin{pmatrix} l' & l & l'' \\ m & -m & 0 \end{pmatrix} \frac{K_{l''+1/2}(2\kappa d)}{\sqrt{\pi\kappa d}}, \quad (10)$$

$$U_{lm'l'm}^{\text{ME}} = -U_{lm'l'm}^{\text{EM}} = (-1)^{l+l'+1} 2i\kappa d m \sum_{l''=|l-l'|}^{l+l'} \times (-1)^{l''} \sqrt{\frac{(2l+1)(2l'+1)}{l(l+1)l'(l'+1)}} (2l''+1) \begin{pmatrix} l' & l & l'' \\ 0 & 0 & 0 \end{pmatrix} \times \begin{pmatrix} l' & l & l'' \\ m & -m & 0 \end{pmatrix} \frac{K_{l''+1/2}(2\kappa d)}{\sqrt{\pi\kappa d}}. \quad (11)$$

Using this result and the T -matrix elements of Eq. (4) we obtain for the interaction energy the large distance expansion

$$E = -\frac{\hbar c}{\pi} \left[\frac{9}{16} \frac{R^3}{d^4} + \frac{25}{32} \frac{R^5}{d^6} + \mathcal{O}(R^6/d^7) \right] \quad (12)$$

at zero temperature.¹⁵

B. Plasma model

We now assume that both the sphere and the plate are described by the plasma model which on the imaginary frequency axis has the dielectric function

$$\epsilon_p(i\kappa) = 1 + \left(\frac{2\pi}{\lambda_p \kappa} \right)^2 \quad (13)$$

and $\mu(i\kappa) = 1$. The plasma wavelength λ_p is related to the plasma frequency ω_p by $\lambda_p = 2\pi c / \omega_p$. Note that the plasma

model provides a high-frequency description of optical properties and ignores dissipation. Hence it is not expected to capture the low-frequency response of a metal.

To understand the physical meaning of the results for the Casimir interaction presented below, it is interesting to realize that the dielectric function of Eq. (13) appears also in the wave equation for the magnetic field in a superconductor when it is described by the London theory. The second London equation and the Maxwell equations yield ϵ_p with the penetration depth $\lambda_p = \sqrt{m_e c^2 / (16\pi^3 n_s e^2)}$ for superfluid carriers of density n_s , charge e , and mass m_e .

To obtain the large distance behavior of the Casimir energy, we need to expand the T matrices for small κ . To this end, we set $\kappa = u/d$ and expand the relevant expressions in powers of $1/d$, where d is compared to the relevant length scales of the model under consideration, see below. The T -matrix elements of the sphere scale as κ^{2l+1} for $\kappa \rightarrow 0$ for both E and M polarizations. In the case of the E polarization the coefficients are universal and are given by the perfect reflector result which corresponds to

$$T_{s,lm}^{\text{E}} = \frac{l+1}{l} \frac{1}{(2l+1)!!(2l-1)!!} (uR/d)^{2l+1} + \dots \quad (14)$$

However, for the M polarization the coefficients are not universal and depend on the plasma wavelength as follows:

$$T_{s,lm}^{\text{M}} = \frac{I_{l+3/2}(2\pi R/\lambda_p)}{I_{l-1/2}(2\pi R/\lambda_p)} \frac{1}{(2l+1)!!(2l-1)!!} (uR/d)^{2l+1} + \dots \quad (15)$$

In the limit of a small plasma wavelength, $\lambda_p \ll R$, the elements of this matrix approach the perfect reflector limit with is given by

$$T_{s,lm}^{\text{M}} = \frac{1}{(2l+1)!!(2l-1)!!} (uR/d)^{2l+1} + \dots \quad (16)$$

For a large plasma wavelength, $\lambda_p \gg R$, the elements are not universal and reduced by a factor $(R/\lambda_p)^2$ compared to the perfect reflector limit,

$$T_{s,lm}^{\text{M}} = \frac{(2\pi R/\lambda_p)^2}{(2l+1)!!(2l+3)!!} (uR/d)^{2l+1} + \dots \quad (17)$$

The latter result can be understood in terms of the London superconductor interpretation of the plasma model. If the penetration depth λ_p becomes much larger than the radius, the sphere becomes almost transparent for the magnetic field and the T -matrix elements are reduced to small values $\sim R^{2l+3}/\lambda_p^2$.

The T -matrix elements of the plate with $\epsilon_p(i\kappa)$ of Eq. (13) and $\mu(i\kappa) = 1$ depend also on the lateral wave vector \mathbf{k}_{\parallel} . To obtain the large distance expansion, we set $k_{\parallel} = v/d$ and expand the T matrix for large d with $z = k_{\parallel} / \kappa = v/u$ fixed. This yields the expansion of the plate's T -matrix elements,

$$T_p^{\text{M}} = 1 - \frac{\sqrt{z^2 + 1} u \lambda_p}{\pi d} + \frac{(z^2 + 1) u^2 \lambda_p^2}{2\pi^2 d^2} + \mathcal{O}[(\lambda_p/d)^3],$$

$$T_p^E = 1 - \frac{u\lambda_p}{\pi d\sqrt{z^2+1}} + \frac{u^2\lambda_p^2}{2\pi^2 d^2(z^2+1)} + \mathcal{O}[(\lambda_p/d)^3]. \quad (18)$$

With this expansion, the integral over z in Eq. (6) can be performed analytically, and one obtains an expansion in $1/d$ of the matrix elements of U which depend on u and λ_p/d only. When we substitute the matrix elements of Eqs. (14), (15), and (18) into Eq. (3) and expand the energy of Eq. (1) in powers of $1/d$, we obtain the interaction to order $1/d^6$ by including $l=2$ partial waves. The result can be written as

$$\mathcal{E} = -\frac{\hbar c}{\pi} \left[f_4(\lambda_p/R) \frac{R^3}{d^4} + f_5(\lambda_p/R) \frac{R^4}{d^5} + f_6(\lambda_p/R) \frac{R^5}{d^6} + \mathcal{O}(R^6 d^{-7}) \right] \quad (19)$$

with the functions

$$f_4(z) = \frac{9}{16} + \frac{9}{64\pi^2} z^2 - \frac{9}{32\pi} z \coth \frac{2\pi}{z}, \quad (20a)$$

$$f_5(z) = -\frac{13}{20\pi} z - \frac{21}{80\pi^3} z^3 + \frac{21}{40\pi^2} z^2 \coth \frac{2\pi}{z}, \quad (20b)$$

$$f_6(z) = \frac{1}{1792[2 \coth(2\pi/z) - z/\pi]} \left\{ \left(2800 + \frac{2595}{\pi^4} z^4 + \frac{10\,072}{\pi^2} z^2 \right) \coth(2\pi/z) - \frac{z/\pi}{\sinh^2(2\pi/z)} \left[-2100 - \frac{285}{\pi^4} z^4 - \frac{223}{\pi^2} z^2 + \left(3780 + \frac{285}{\pi^4} z^4 + \frac{3763}{\pi^2} z^2 \right) \cosh(4\pi/z) - \frac{1260}{\pi} z \coth(2\pi/z) \right] \right\}. \quad (20c)$$

Note the coefficient f_4 of the leading term depends on λ_p of the *sphere only* and hence is not universal. Only in the two limits $\lambda_p/R \rightarrow 0$ and $\lambda_p/R \rightarrow \infty$ the coefficient approaches the material independent values $9/16$ and $3/8$, respectively. This behavior is consistent with the two limiting forms of the sphere's T matrix of Eqs. (16) and (17). The limit $\lambda_p/R \rightarrow 0$ describes perfect reflection of electric and magnetic fields at arbitrarily low frequencies and hence agrees with the result of Eq. (12) where for dipole fluctuations the E polarization yields twice the contribution of the M polarization, cf. Eqs. (14) and (16) for $l=1$. For $\lambda_p/R \rightarrow \infty$ the coefficient f_4 is reduced by a factor $2/3$ since the M polarization does not contribute to the leading term $\sim R^3/d^4$ due its suppression by $(R/\lambda_p)^2$, cf. Eq. (17). Physically, the nonuniversal behavior of f_4 can be understood when the objects are considered as London superconductors. For $\lambda_p/R \rightarrow 0$ a static magnetic field is perfectly screened and the objects become perfect reflectors. If $\lambda_p/R \gg 1$, a static magnetic field can penetrate the entire sphere and hence the M polarization does not contribute to the Casimir energy. From this interpretation it follows that normal metals, which can be penetrated by a static magnetic field, should interact to leading order in R/d

only via E polarizations leading to $f_4=3/8$. We shall reach the same conclusion when we consider the Drude model below. The coefficient of R^4/d^5 depends on λ_p of both the sphere and the plate. It is always positive and varies between $(13/20\pi^2)(\lambda_p/R)$ for $\lambda_p/R \rightarrow 0$ and $(3/10\pi^2)(\lambda_p/R)$ for $\lambda_p/R \rightarrow \infty$. The coefficient of R^5/d^6 can be negative (for $\lambda_p/R \rightarrow 0$) or positive. The validity range of the expansion of Eq. (19) is determined by $d \gg R$ and $d \gg \lambda_p$ so that the corrections to the first term are small. In Sec. V, we compare the exact findings of Sec. V to our results from a numerical evaluation of Eq. (2) over a wide range of separations.

Finally, it is instructive to compare the above results to the interaction between two parallel and infinite plates that are described by the plasma model. In this case, the large distance expansion applies to $d \gg \lambda_p$ and the leading term is given by the universal perfect reflector result. The plasma wavelength appears only in corrections to the leading term that can be expanded in powers of λ_p/d . This universal behavior is a consequence of the (unrealistic) assumption of an infinite lateral size of the plates which removes any finite length scale of the object that could be compared to λ_p . Hence, a finite penetration depth only yields an increased effective separation which for $d \gg \lambda_p$ obviously approaches d , explaining the universal large- d result.

C. Drude model

The Drude model describes the low-frequency response of a metal which depends on its dc conductivity σ . For large frequencies it becomes identical to the plasma model with plasma wavelength λ_p . On the imaginary frequency axis, the Drude dielectric function is given by

$$\epsilon_D(ic\kappa) = 1 + \frac{(2\pi)^2}{(\lambda_p\kappa)^2 + \pi c\kappa/\sigma} \quad (21)$$

and $\mu(ic\kappa)=1$. The conductivity is associated with the length scale $\lambda_\sigma=2\pi c/\sigma$. At large distances d , we need to consider the limit of small κ at fixed $z=k_{\parallel}/\kappa$ for the plate's T matrix, which yields with $\kappa=u/d$,

$$T_p^M = 1 - \sqrt{\frac{uc}{\pi d\sigma}} \sqrt{z^2+1} + \frac{uc}{2\pi d\sigma} (z^2+1) + \mathcal{O}[(c/d\sigma)^{3/2}], \quad (22a)$$

$$T_p^E = 1 - \sqrt{\frac{uc}{\pi d\sigma}} \frac{1}{\sqrt{z^2+1}} + \frac{uc}{2\pi d\sigma} \frac{1}{z^2+1} + \mathcal{O}[(c/d\sigma)^{3/2}]. \quad (22b)$$

The approach of unity for both polarizations is a consequence of keeping k_{\parallel}/κ fixed in the limit $\kappa \rightarrow 0$. This behavior arises from the fact that the plates are infinitely extended so that arbitrarily small k_{\parallel} are allowed. The situation is different at finite temperatures where one has to take $\kappa \rightarrow 0$ at fixed k_{\parallel} for the first term of the sum over Matsubara frequencies. In the latter limit the magnetic contribution T_p^M vanishes.

For the sphere with the Drude dielectric function of Eq. (21) and $\mu(ic\kappa)=1$ we obtain for the T -matrix elements with $l=1$ the low-frequency expansion

$$T_{s,1m}^M = \frac{4\pi R\sigma}{45c} (uR/d)^4 + \dots, \quad (23a)$$

$$T_{s,1m}^E = \frac{2}{3} (uR/d)^3 - \frac{1}{2\pi R\sigma} c (uR/d)^4 + \dots. \quad (23b)$$

While the leading term of the E polarization agrees with the perfect reflector result, the leading term of the M polarization is reduced by a factor $R\kappa=uR/d$ compared to the perfect reflector case. Therefore, one expects that only the E polarization contributes to the leading term of the interaction at large distances.

With the above expansion of the T -matrix elements the integrations over u and z can be performed and from the dipole contributions with $l=1$ we obtain for the energy the large distance expansion

$$E = -\frac{\hbar c}{\pi} \left[\frac{3R^3}{8d^4} - \frac{77}{384} \frac{R^3}{\sqrt{2\sigma/c}d^{9/2}} - \frac{cR^3}{8\pi\sigma d^5} + \frac{\pi\sigma R^5}{20cd^5} + \mathcal{O}(R^3\lambda_\sigma^{3/2}d^{-11/2}, R^5\lambda_\sigma^{-1/2}d^{-11/2}) \right]. \quad (24)$$

The leading term in Eq. (24) shows the universal amplitude coming only from the E polarization as expected from the form of the T -matrix elements. This result reproduces the prediction of the plasma model in the limit where $\lambda_p \gg R$, see the discussion below Eq. (20a). This limit describes the situation where a static magnetic field can fully penetrate the sphere and hence describes a normal metal. The correlations between material and shape become obvious when one compares the above result to the interaction between two parallel and infinite plates that are described by the Drude model. For this geometry the large distance expansion applies to $d \gg c/\sigma$. The leading term of this expansion is identical to the perfect reflector result, as for the plasma model. The dc conductivity appears only in corrections to the leading term that can be expanded in integer powers of $\sqrt{c/\sigma}d$. Since the frequently used PFA for the sphere-plate geometry is based on the two-plate energy, it would predict at sufficiently large d for both the plasma and the Drude model the perfect reflector result which has equal contributions from E and M polariza-

tion. However, it is known that the PFA does not apply to large distances. It should be noted that the result of Eq. (24) cannot be applied to an arbitrarily large dc conductivity σ since then the term $\sim R^5$, which comes from the M polarization of the sphere, diverges. The condition for the validity of Eq. (24) can be written as $d \gg R, \lambda_\sigma, \lambda_p, R^2/\lambda_\sigma$. Below we shall study the validity range of this expansion further by comparing it to numerical results.

IV. HIGH-TEMPERATURE LIMIT

In this section, we study the high-temperature limit of the sphere-plate interaction for the plasma and Drude model. In this case, the interaction is given by the first term of the Matsubara sum of Eq. (1). Hence we have to compute the matrix elements of $Y(\kappa_0=0)$. This zero-frequency result will turn out to be also useful when computing the Casimir energy at zero and finite temperatures below since the limit $\kappa \rightarrow 0$ is numerically unstable due to the divergence of certain Bessel functions.

A. Plasma model

Here we have to consider the limit $\kappa \rightarrow 0$ at fixed k_\parallel of the T matrix of the plate since we are interested in arbitrary separations d . In this limit the T -matrix elements are given by

$$T_p^M = -\frac{|k_\parallel| - \sqrt{4\pi^2/\lambda_p^2 + k_\parallel^2}}{|k_\parallel| + \sqrt{4\pi^2/\lambda_p^2 + k_\parallel^2}}, \quad T_p^E = 1. \quad (25)$$

The elements for the M polarization are nonuniversal and vary between 1 for $\lambda_p \rightarrow 0$ (perfect reflector) and 0 for $\lambda_p \rightarrow \infty$. The latter limit can be interpreted as a London superconductor with diverging penetration depth such that the plate is transparent to a static magnetic field.

For $\lambda_p \rightarrow 0$ the U matrix of Eq. (6) can be obtained for $\kappa \rightarrow 0$ from Eq. (10). To obtain the U matrix for $\kappa \rightarrow 0$ at nonzero but small $\lambda_p \ll d$, we set $k_\parallel = v/d$ and expand T_p^M of Eq. (25) in λ_p/d so that the integral of Eq. (6) can be performed analytically. Since we are interested in the limit $\kappa \rightarrow 0$, we only need the conversion matrix elements $D_{lm}^{\alpha\gamma}(z)$ for large arguments z . At large z the associated Legendre polynomials $P_{lm}(z)$ assume the limiting form $(-i)^m (2l-1)!! z^l / (l-m)!$. Using the integral $\int_0^\infty e^{-2v} v^n dv = n! / 2^{n+1}$ we obtain to leading order for small κ the matrix elements

$$U_{lm'l'm}^{EE} = \sqrt{\frac{l(2l+1)l'(2l'+1)}{(l+1)(l'+1)}} \frac{(2l-1)!!(2l'-1)!!(l+l')!}{\sqrt{(l+m)!(l-m)!(l'+m)!(l'-m)!}} \frac{1}{(2\kappa d)^{l+l'+1}}, \quad (26a)$$

$$U_{lm'l'm}^{MM} = U_{lm'l'm}^{EE} \left\{ 1 - \frac{l+l'+1}{2\pi} \frac{\lambda_p}{d} + \mathcal{O}[(\lambda_p/d)^2] \right\}. \quad (26b)$$

The matrix elements $U_{lm'l'm}^{EM}, U_{lm'l'm}^{ME}$ scale for small κ as $(\kappa d)^{-l-l'}$ and hence can be ignored. The T -matrix elements of the sphere for $\kappa \rightarrow 0$ are given by Eqs. (14) and (15) and hence scale as κ^{2l+1} . The low- κ scaling of the matrix elements of U and T_s shows that the elements of the matrix Y scale as $Y_{lm'l'm}^{EE} \sim Y_{lm'l'm}^{MM} \sim \kappa^{l-l'}$ and $Y_{lm'l'm}^{EM} \sim Y_{lm'l'm}^{ME} \sim \kappa^{l-l'+1}$. Hence for $\kappa \rightarrow 0$ the

coupling of E and M polarization does not contribute to the energy. We set again $\kappa=u/d$ and introduce the rescaled matrix \tilde{Y} with elements $\tilde{Y}_{lm'l'm'}=u^{-l}Y_{lm'l'm}u^{l'}$ so that divergences for $u\rightarrow 0$ are removed and in that limit all elements of \tilde{Y}^{MM} and \tilde{Y}^{EE} assume nonzero finite values that depend on R/d and λ_p/d , and all elements of \tilde{Y}^{ME} and \tilde{Y}^{EM} vanish. The rescaling does not change the determinant of Eq. (1) so that $\det Y=\det \tilde{Y}$. In the high-temperature limit the energy can then be written as

$$E = \frac{k_B T}{2} \log \det \begin{pmatrix} 1 - \tilde{Y}^{\text{MM}}(u \rightarrow 0) & 0 \\ 0 & 1 - \tilde{Y}^{\text{EE}}(u \rightarrow 0) \end{pmatrix}, \quad (27)$$

where the matrix elements of \tilde{Y} are given by Eqs. (3), (14), (15), and (26). By truncating the matrix \tilde{Y} at lowest order $l=1$ we get the high-temperature free energy

$$E = -k_B T \left\{ \left[\frac{3}{8} + \frac{3}{32\pi^2} \frac{\lambda_p^2}{R^2} - \frac{3}{16\pi} \frac{\lambda_p}{R} \coth\left(2\pi \frac{R}{\lambda_p}\right) \right] \frac{R^3}{d^3} - \left[\frac{3}{16\pi} \frac{\lambda_p}{R} + \frac{9}{64\pi^3} \frac{\lambda_p^3}{R^3} - \frac{9}{32\pi^2} \frac{\lambda_p^2}{R^2} \coth\left(2\pi \frac{R}{\lambda_p}\right) \right] \frac{R^4}{d^4} + \mathcal{O}((R/d)^5) \right\}, \quad (28)$$

which applies for $d \gg R$, λ_p , $\lambda_T = \hbar c / k_B T$. Notice that this energy is not universal in the sense that the leading term depends on the plasma wavelength. For $\lambda_p \ll R$, the amplitude of the leading term becomes $-3/8$, in agreement with the high-temperature result for perfect reflectors.¹⁷ For $\lambda_p \gg R$, the amplitude of the leading term approaches $-1/4$ which is identical to the result for the Drude model [see Eq. (27) below]. The behavior in these two limits is consistent with the corresponding limits of the zero-temperature result of Eq. (19).

B. Drude model

For this model, the T matrix of the plane for $\kappa \rightarrow 0$ at fixed k_{\parallel} behaves differently from Eq. (21). While $T_p^E \rightarrow 1$, the magnetic part vanishes, $T_p^M \rightarrow 0$. Equation (6) shows that to leading order for small κ , the matrix elements $U_{lm'l'm}^{\text{EE}}$ are given by Eq. (26). In fact, we do not need to find the other matrix elements of U : the elements coupling unlike polarizations are reduced by a factor κ , and the elements $U_{lm'l'm}^{\text{MM}}$ are multiplied by $T_{s,lm}^M$ of the sphere, which scales as κ^{2l+2} for small values of κ , and are thus smaller by a factor κ also. The (universal) elements of $T_{s,lm}^E$ for small κ are given by Eq. (14). This shows that only the E polarization contributes to the energy at high temperatures and from Eqs. (14) and (26) follows the explicit result for the elements of the rescaled matrix \tilde{Y}^{EE} ,

$$\lim_{u \rightarrow 0} \tilde{Y}_{lm'l'm}^{\text{EE}}(u) = \frac{l+1}{l} \frac{1}{2^{l+l'+1}} \sqrt{\frac{l(2l+1)l'(2l'+1)(2l'-1)!!(l+l')!}{(l+1)(l'+1)(2l+1)!!}} \frac{(R/d)^{2l+1}}{\sqrt{(l+m)!(l-m)!(l'+m)!(l'-m)!}}. \quad (29)$$

In the high-temperature limit the energy is then given by

$$E = \frac{k_B T}{2} \log \det [1 - \tilde{Y}^{\text{EE}}(u \rightarrow 0)]. \quad (30)$$

Notice that this result is universal at *all* separations since the matrix \tilde{Y} depends only on R/d . The absence of magnetic contributions is in agreement with the high-temperature interaction between two parallel plates that are described by the Drude model. A truncation of the matrix \tilde{Y} at $l=2$ and expansion of Eq. (30) for small R/d yields the large distance result

$$E = -k_B T \left[\frac{1}{4} \left(\frac{R}{d}\right)^3 + \frac{1}{4} \left(\frac{R}{d}\right)^5 + \frac{3}{128} \left(\frac{R}{d}\right)^6 + \mathcal{O}\left(\frac{R^7}{d^7}\right) \right] \quad (31)$$

which applies when $d \gg R$, λ_T .

V. NUMERICS

In this section, we evaluate the Casimir energy based on Eq. (2) for zero temperature and Eq. (1) for finite temperatures. Our results are obtained by numerical computation of the determinant, the integral over κ (or sum over n) and the integral over z of Eq. (6). The matrix Y is truncated at a finite partial wave order, ℓ_{max} . We chose ℓ_{max} such that the result for the energy changes by less than a factor of 1.0001 upon increasing ℓ_{max} by 10. The required value of ℓ_{max} depends on the separation between the plate and sphere. As the separation decreases, ℓ_{max} increases. For example, for $R/d < 0.75$, we used $\ell_{\text{max}}=24$, whereas for $R/d=0.8$ and 0.85 , one needs $\ell_{\text{max}}=34$ and for $R/d=0.9$ the value $\ell_{\text{max}}=54$.

The numerical computation of the determinant, the integrals and sum poses no principle problem. However, it is important to consider the determinant of Eq. (1) and (2) carefully for $\kappa \rightarrow 0$. In Sec. IV we have already seen that the matrix elements $Y_{lm'l'm}$ for small κ scale as $\kappa^{l-l'}$ or $\kappa^{l-l'+1}$. This shows that for small κ the matrix elements with $l \gg l'$

become extremely small whereas those with $l \ll l'$ increase rapidly. For large values of l_{max} this behavior makes the computation of the determinant at $\kappa=0$ numerically ill conditioned. However, the analytical results presented in Sec. IV allow us to calculate the $n=0$ term in Eq. (1) or the integrand of Eq. (2) at $\kappa=0$ for $l_{max}=100$ and even larger. In fact, as the value of R/d is increased beyond 0.9, larger values $l_{max} > 60$ must be used in order to accurately calculate the energy. For sufficiently high temperatures, the second Matsubara wave vector $\kappa_1 = 2\pi k_B T / \hbar c$ in Eq. (1) becomes sufficiently large and hence poses no numerical problem for the computation of the energy. For example, for $T=300$ K the Casimir energy can be calculated for $R/d=0.95$ with $l_{max}=72$. As l_{max} increases, the interval in the vicinity of $\kappa=0$ in which the integrand cannot be obtained with sufficient precision numerically increases too. Due to this behavior, we restrict the calculation of the Casimir energy at $T=0$ to $R/d \leq 0.9$.

A. Casimir interaction at $T=0$

In this section, we calculate the Casimir energies for the usual Drude and plasma model given in Eqs. (13) and (21), respectively, for parameters of gold as given below. There are three dimensionless parameters which we choose as d/R , λ_p/R , and λ_p/λ_σ . The first two parameters can be controlled for a given material by changing the separation d and the radius R of the sphere. In order to avoid strong finite size effects in the electronic response, we assume that $\lambda_\sigma, \lambda_p < R$.

In Secs. III B and III C, using $l_{max}=2$ partial waves, we obtained an asymptotic expansion of the Casimir energy for both plasma and Drude model at large separations, see Eqs. (19) and (24). In Fig. 1, we compare the analytical results to the exact numerical results that were obtained as described before. The graph shows the exact energies for the Drude and the plasma model normalized to the exact energies for perfect reflecting surfaces, taken from Ref. 15. For the plasma model we used $\lambda_p/R=0.05$ and 0.5, respectively, and for the Drude model the same two values for λ_p/R and we set $\lambda_p/\lambda_\sigma=27.4$, corresponding to gold for which $\lambda_p=137$ nm and $\lambda_\sigma \approx 5$ nm. The figure illustrates the material dependence of the Casimir energies. For large separations, the ratios for the plasma model approach values slightly smaller than one, which is consistent with the λ_p/R -dependent asymptotic form predicted by Eq. (19). For the case of the Drude model, the ratio tends to the universal number $2/3$ at large separations, as predicted by Eqs. (12) and (24). In the case of the plasma model, the asymptotic result describes the energy up to $R/d \approx 0.4$ nicely. For the Drude model, however, the agreement between the analytical and numerical findings is limited to extremely small $R/d \leq 10^{-4}$. This example clearly indicates distinct correlations between material and geometry. The large deviation of the analytical results from the numerical data at intermediate distances shows that for the Drude model a larger number of partial waves than for the plasma model is necessary to accurately calculate the Casimir energy.

We also compare the exact numerical results with the Casimir energy obtained by the PFA for both the plasma and the

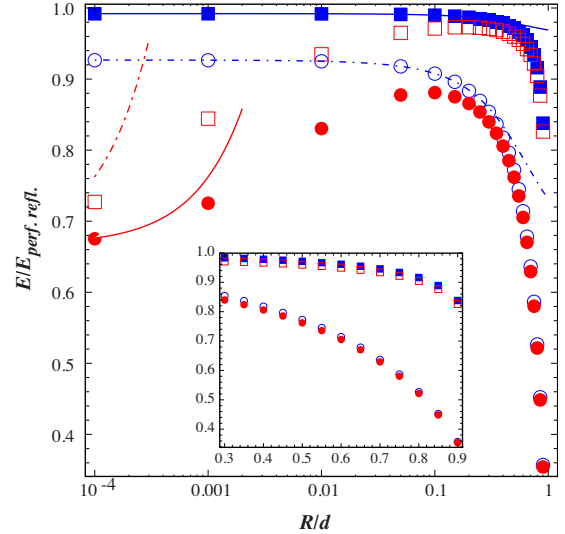


FIG. 1. (Color online) $E/E_{\text{perf. refl.}}$ against R/d for the plasma model for $\lambda_p/R=0.5, 0.05$ (open circles and filled squares, respectively), and the Drude model for the same values of λ_p/R (filled circles and open squares, respectively) and $\lambda_p/\lambda_\sigma=27.4$, corresponding to gold. The solid and dashed lines represent the asymptotic results of Eqs. (19) and (24) for the plasma and the Drude model, respectively. Inset: magnification of the short distance range.

Drude model. The PFA energy is obtained by integrating the PFA force $F=2\pi RE_{\text{plates}}(d-R)$ with respect to d , where $E_{\text{plates}}(d-R)$ is the energy of two parallel plates at distance $d-R$ as given by the Lifshitz formula²³ with the corresponding dielectric function. Figure 2 shows the exact Casimir energy calculated numerically for the plasma model with plasma wavelength $\lambda_p/R=0.05$ and $\lambda_p/R=0.5$, respectively. The figure shows also the PFA energy for the same values of λ_p . As expected, the discrepancy between the exact and PFA energy decreases as R/d increases and is expected to vanish for $d \rightarrow R$. This is clearly visible from Fig. 3 which shows the relative corrections to the PFA energy at short separations. Interestingly, the dependence of the corrections on λ_p is not fully described by the Lifshitz theory since the data for different λ_p do not collapse onto a single curve. This demon-

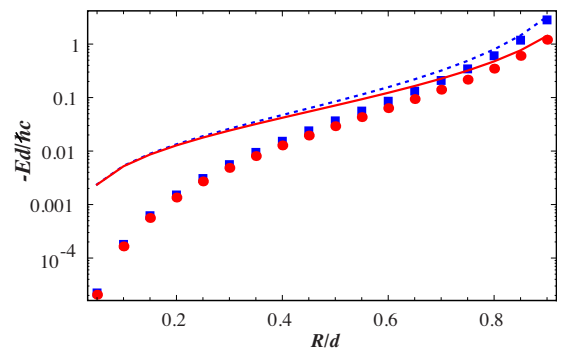


FIG. 2. (Color online) Numerical result for $-Ed/\hbar c$ against R/d for the plasma model at $\lambda_p/R=0.05$ (squares) and at $\lambda_p/R=0.5$ (circles). The lines represent the PFA energy at $\lambda_p/R=0.05$ (dashed) and at $\lambda_p/R=0.5$ (solid).

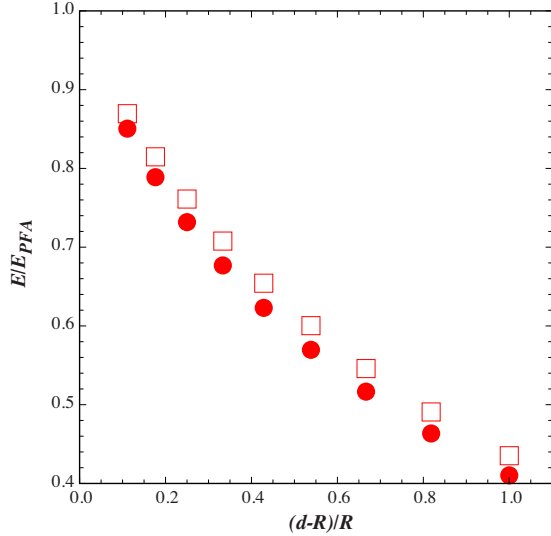


FIG. 3. (Color online) Ratio of the numerical results for the Casimir energy shown in Fig. 2 and the PFA energy based on the Lifshitz theory for the plasma model with $\lambda_p/R=0.05$ (squares) and $\lambda_p/R=0.5$ (circles). The ratio is shown as a function of the surface-to-surface distance $d-R$.

strates correlations between geometry and material properties that are not described by the PFA.¹⁶ For example, for $\lambda_p/R=0.5$ and $\lambda_p/R=0.05$ we find at the shortest studied separation of $d-R=0.11R$ the exact energy to be 85% and 87% of the PFA energy, respectively. For perfect reflectors the reduction was found to be $\approx 87\%$ at the same distance.¹⁵ We find similar results using the Drude model. The energies associated with the Drude model are not shown here since they collapse onto the data for the plasma model at short separations.

B. Casimir interaction at $T \neq 0$

The Casimir free energy at finite temperatures T depends on the thermal wavelength $\lambda_T = \hbar c / k_B T$. This additional length scale introduces an additional dimensionless parameter λ_T/R . To investigate the influence of temperature, we calculated the Casimir free energy at two different values of this parameter. We have chosen the values $\lambda_T/R=1.52, 5.94$ since they correspond, e.g., to a sphere of radius $R=5 \mu\text{m}$, which is small but still relevant to experiments. The temperature is chosen as $T=300 \text{ K}$ and $T=77 \text{ K}$, yielding $\lambda_T=7.6 \mu\text{m}$ and $\lambda_T=29.7 \mu\text{m}$, respectively. These two temperatures, corresponding to room temperature and the boiling point of molecular nitrogen N_2 , respectively, can readily be accessed in experiments.

Below, we employ more detailed models for the material response to calculate the Casimir energies at higher temperatures. More specifically, we consider generalized plasma and Drude models, which take into account the interband transitions of core electrons that are described by a set of oscillators with nonzero resonant frequencies. The generalized plasma model has the dielectric permittivity

$$\epsilon_p(i c \kappa) = 1 + \left(\frac{2\pi}{\lambda_p \kappa} \right)^2 + \epsilon_c(i c \kappa) \quad (32)$$

and the generalized Drude is described by

TABLE I. Oscillator parameters for gold. Calculated in Ref. 5 by fitting six oscillators to tabulated optical data (Ref. 24).

j	ω_j (eV)	g_j (eV)	f_j (eV ²)
1	3.05	0.75	7.091
2	4.15	1.85	41.46
3	5.4	1.0	2.700
4	8.5	7.0	154.7
5	13.5	6.0	44.55
6	21.5	9.0	309.6

$$\epsilon_p(i c \kappa) = 1 + \frac{(2\pi)^2}{(\lambda_p \kappa)^2 + \pi c \kappa / \sigma} + \epsilon_c(i c \kappa) \quad (33)$$

with

$$\epsilon_c(i c \kappa) = \sum_{j=1}^K \frac{f_j}{\omega_j^2 + (c \kappa)^2 + g_j c \kappa} \quad (34)$$

and we set again $\mu(i c \kappa)=1$. Here K is the number of oscillators, f_j are the oscillator strengths, g_j are the relaxation frequency, and $\omega_j \neq 0$ are the resonant frequencies of the core electrons. Typical parameters for gold are given by $\omega_p=9 \text{ eV}$ for the plasma frequency and $\gamma=35 \text{ meV}$ for the relaxation rate.¹⁶ These parameters correspond to the length scales $\lambda_p=2\pi c / \omega_p=137 \text{ nm}$ and $\lambda_\gamma=2\pi c / \gamma=35.4 \mu\text{m}$. For these parameters, the dc conductivity $\sigma=\omega_p^2 / (4\pi\gamma)$ is 184.2 eV, corresponding to the length scale $\lambda_\sigma=2\pi c / \sigma=6.7 \text{ nm}$. Note that electron scattering is not described by the usual plasma model. However, as can be seen from Eq. (32), dissipation is included in the generalized plasma model due to the interband transition of core electrons. To calculate the Casimir energy, we use the oscillator parameters of gold which are presented in Table I. These parameters have been calculated⁵ based on the six-oscillator model fitted to the tabulated optical data given in Ref. 24.

We first calculated the $n=0$ term of the sum of Eq. (1) analytically, based on the expressions given in Sec. IV and then calculate the other terms numerically as explained previously. This allows us to calculate the Casimir free energy for very short separations. As explained above, large values of ℓ_{max} should be used at short separations but in this limit the numerical evaluation of the determinant in Eq. (1) is cumbersome. This problem disappears as the temperature is increased because then the second Matsubara wave vector κ_1 becomes larger and thus no calculation for too small values of $\kappa > 0$ will be necessary. For the purpose of this paper, we calculate the relevant energies for distances as short as $R/d=0.95$ at the two different temperatures using the generalized form of the Drude and the plasma model, see Eqs. (32) and (33).

Figure 4 shows the ratio of the Casimir free energy to the energy at $T=0$ for the generalized plasma model and for the generalized Drude model at $T=300 \text{ K}$ and $T=77 \text{ K}$. While the Casimir free energy at $T=300 \text{ K}$ is always larger than at $T=77 \text{ K}$ for the plasma model, we find that for the Drude

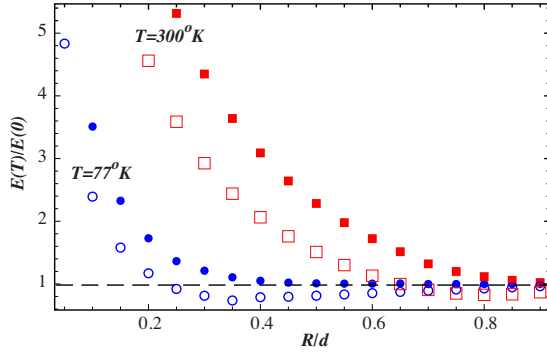


FIG. 4. (Color online) Ratio of the Casimir free energy to the energy at $T=0$ against R/d for the generalized Drude model (open symbols) and the generalized plasma model (filled symbols) at $T=300$ K (squares) and at $T=77$ K (circles) for a sphere of radius $R=5 \mu\text{m}$.

model the Casimir free energies at $T=77$ K and $T=300$ K cross each other around $R/d=0.7$. For $R/d \geq 0.7$, the Casimir free energy corresponding to $T=77$ K becomes larger than the one for $T=300$ K. For the sphere plate geometry, indications of negative entropy have recently been reported.¹⁷ The ratio shown in Fig. 4 can be expressed as $E(T)/E(0)=1 - TS/E(0)$, where S is the entropy associated with the Casimir free energy $E(T)$. Hence, a ratio $E(T)/E(0) < 1$ implies a negative entropy since $E(0) < 0$. Our results clearly show that for the Drude model the entropy indeed becomes negative for sufficiently small separations. However, for the plasma model our results of Fig. 4 indicate a positive entropy.

Above we showed that at large separations the ratio of the Casimir energy for the plasma and the Drude model varies between $3/2$ (for small λ_p/R) and 1 (for large λ_p/R) for zero and finite temperatures. At shorter separations the ratio is expected to tend to one since at high frequencies the plasma and Drude model become identical. It is interesting to observe how the ratio tends to one with decreasing separation as a function of temperature. Figure 5 shows the Casimir free energy for the plasma model divided by that for the Drude model at $T=300$ K, $T=77$ K, and $T=0$ K. Since $\lambda_p/R = 0.0274$ is small compared to one, the ratio tends to almost $3/2$ at large separations. As shown in the figure, with decreasing

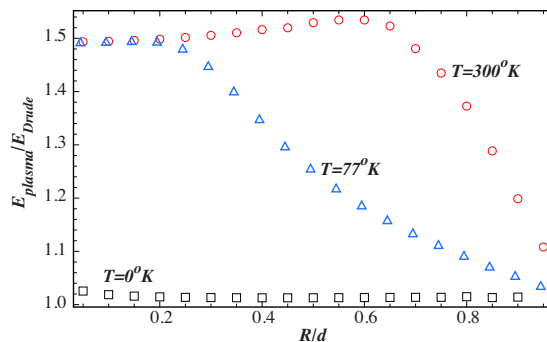


FIG. 5. (Color online) The ratio of Casimir free energies for the generalized plasma and generalized Drude model at $T=300$ K (circles), $T=77$ K (triangles), and $T=0$ (squares).

ing separation the ratio drops toward one very fast for $T=0$. However, for $T=300$ K the ratio is larger than $3/2$ for $R/d \leq 0.7$, goes through a maximum around $R/d=0.6$, and finally starts dropping to one. The curve for $T=77$ K also displays a slight maximum close to $R/d=0.15$. A similar behavior with an extrema has been observed also in Ref. 17 for a sufficiently large sphere at $T=300$ K. The maxima occur at a distance that approximately corresponds to the thermal wavelength λ_T with $R/\lambda_T=0.66$ and $R/\lambda_T=0.17$ for $T=300$ K and $T=77$ K, respectively. Since thermal photons of wavelength λ_T mostly contribute to the energy at a separation $d \approx \lambda_T$, the position of the maxima suggests that thermal effects less strongly enhance the Drude energy than the plasma energy, presumably due to dissipation.

VI. CONCLUSION

We have shown in detail how the scattering approach for Casimir interactions can be applied to study correlations between effects due to geometry, material properties, and finite temperature. The experimentally most relevant geometry of a sphere and plate reveals interesting properties of the Casimir interaction that are absent for parallel plates and hence in the proximity force approximation. These findings demonstrate an interplay between material properties and the finite size of the sphere. Our main results are as follows. At large separations we observe both at zero and finite temperatures for the amplitude of the leading term of the energy different results for perfect reflectors, Drude, and plasma metals. The plasma model yields a nonuniversal amplitude that depends on the ratio of plasma wavelength to sphere radius. For the perfect reflector and Drude model the amplitudes are universal but for the latter it is reduced by a factor of $2/3$. This result is distinct from the interaction of two parallel plates, which at zero temperature is asymptotically identical for the three material descriptions. The identification of the plasma wavelength with the penetration depth of a London superconductor explains why the plasma model yields the asymptotic interaction for perfect reflectors and a Drude metals as limiting cases.

Our numerical computations of the energy at smaller separations demonstrate further important differences between the plasma and Drude model and generalizations thereof. We observe full agreement of the numerical results with the asymptotic expansion at large separations that, however, is limited for the Drude model to extremely large distances. Hence, we conclude that for the Drude model higher-order multipoles are more important than for the plasma model. At small separations the observed dependence of the difference between the exact and the PFA energies on the plasma wavelength demonstrates that geometry and material effects are correlated. Our results at finite temperatures show that the Casimir energy for Drude metals changes nonmonotonically with temperature, leading to a larger energy at $T=77$ K than at $T=300$ K at sufficiently small separations. We observe a negative entropy associated with the Casimir free energy for the Drude model over a range of distances. This range increases when the temperature is decreased. Both nonmonotonic temperature dependence and negative entropy

are not observed for the plasma model in the range of studied parameters. At finite temperatures, we find that the Casimir free energy for plasma metals is approximately $3/2$ times the energy for Drude metals for separations $d \geq \lambda_T$.

ACKNOWLEDGMENTS

The results for large separations at $T=0$ and their interpretation in terms of a London superconductor have been presented before at the QFEXT09 conference at the Univer-

sity of Oklahoma. We thank G. Bimonte, M. Kardar for useful conversations regarding this work. We are grateful to S. J. Rahi for his extensive help on various aspects of this work. This work was supported by the National Science Foundation (NSF) through Grants No. DMR-06-45668 (R.Z.) and No. PHY0653657 (U.M.), U.S. Department of Energy (DOE) through Grant No. DE-FG02-04ER46131, Defense Advanced Research Projects Agency (DARPA) under Contract No. S-000354 (R.Z., T.E., and U.M.), and by the Deutsche Forschungsgemeinschaft (DFG) through Grant No. EM70/3 (T.E.).

-
- ¹S. K. Lamoreaux, *Phys. Rev. Lett.* **78**, 5 (1997).
²U. Mohideen and A. Roy, *Phys. Rev. Lett.* **81**, 4549 (1998).
³B. W. Harris, F. Chen, and U. Mohideen, *Phys. Rev. A* **62**, 052109 (2000).
⁴R. S. Decca, D. Lopez, E. Fischbach, G. L. Klimchitskaya, D. E. Krause, and V. M. Mostepanenko, *Ann. Phys.* **318**, 37 (2005).
⁵R. S. Decca, D. Lopez, E. Fischbach, G. L. Klimchitskaya, D. E. Krause, and V. M. Mostepanenko, *Eur. Phys. J. C* **51**, 963 (2007).
⁶G. L. Klimchitskaya, U. Mohideen, and V. M. Mostepanenko, *Rev. Mod. Phys.* **81**, 1827 (2009).
⁷H. B. G. Casimir, *Proc. K. Ned. Akad. Wet.* **51**, 793 (1948).
⁸I. E. Dzyaloshinskii, E. M. Lifshitz, and L. P. Pitaevskii, *Adv. Phys.* **10**, 165 (1961).
⁹D. E. Krause, R. S. Decca, D. López, and E. Fischbach, *Phys. Rev. Lett.* **98**, 050403 (2007).
¹⁰T. Emig, N. Graham, R. L. Jaffe, and M. Kardar, *Phys. Rev. A* **79**, 054901 (2009).
¹¹S. J. Rahi, T. Emig, N. Graham, R. L. Jaffe, and M. Kardar, *Phys. Rev. D* **80**, 085021 (2009).
¹²M. Bordag, G. L. Klimchitskaya, U. Mohideen, and V. M. Mostepanenko, *Advances in the Casimir Effect* (Oxford University Press, Oxford, 2009).
¹³F. Chen, G. L. Klimchitskaya, V. M. Mostepanenko, and U. Mohideen, *Phys. Rev. B* **76**, 035338 (2007).
¹⁴V. A. Parsegian, *van der Waals Forces* (Cambridge University Press, Cambridge, 2005).
¹⁵T. Emig, *J. Stat. Mech.: Theory Exp.* (2008) P04007.
¹⁶A. Canaguier-Durand, P. A. Maia Neto, I. Cavero-Pelaez, A. Lambrecht, and S. Reynaud, *Phys. Rev. Lett.* **102**, 230404 (2009).
¹⁷A. Canaguier-Durand, Paulo A. Maia Neto, A. Lambrecht, and S. Reynaud, *Phys. Rev. Lett.* **104**, 040403 (2010).
¹⁸T. Emig, R. L. Jaffe, M. Kardar, and A. Scardicchio, *Phys. Rev. Lett.* **96**, 080403 (2006).
¹⁹M. Bordag, *Phys. Rev. D* **73**, 125018 (2006).
²⁰M. Bordag and V. Nikolaev, *Phys. Rev. D* **81**, 065011 (2010).
²¹H. Gies and K. Klingmüller, *Phys. Rev. Lett.* **96**, 220401 (2006).
²²G. Mie, *Ann. Phys.* **330**, 377 (1908).
²³E. M. Lifshitz, *Sov. Phys. JETP* **2**, 73 (1956).
²⁴E. D. Palik, *Handbook of Optical Constants of Solids* (Academic, New York, 1985).